Supplementary Information

Dynamic dissection of NINJ1-mediated plasma membrane rupture reveals a multi-stage process

Zhaoyi Zhai[1,2]†, Xue Bai[3]†, Bo Yan[4,5]†, Zehao Zhou[6]†, Fang Chen[5]†, Xinrui Guo[1,7], Jie Chen[3], Chenguang Yang[1,8], James Daniel Farrell[1,9,10], Rongjing Chen[1,8], Yan Ma[11], Yang Cao[11], Zhen Zhou[5], Xin Liu[7], Qiaozhen Kang[7], Zhongbo Yu[2], Ying Lu[1,8,10], Ming Li[1,8,10], Lijiang Yang[12], Guanghou Shui[5], Xun Huang[5], Yi Qin Gao[6,12,13]*, Youwei Ai[5]*, Zhe Zhang[3,14]*, Fang Jiao[1]*

[1]Beijing National Laboratory for Condensed Matter Physics, Institute of Physics, Chinese Academy of Sciences, Beijing 100190, China.

[2]State Key Laboratory of Medicinal Chemical Biology, College of Pharmacy, Nankai University, Tianjin 300350, China.

[3]State Key Laboratory of Membrane Biology, School of Life Sciences, Peking University, Beijing 100871, China.

[4]Department of Neurology, Tianjin Neurological Institute, Tianjin Medical University General Hospital, Tianjin 300052, China.

[5]Laboratory of Integrative Physiology, Institute of Genetics and Developmental Biology, Chinese Academy of Sciences, Beijing 100101, China.

[6]Changping Laboratory, Beijing 102200, China.

[7]School of Life Sciences, Zhengzhou University, Zhengzhou 450001, China.

[8]University of Chinese Academy of Sciences, Beijing 100049, China.

[9]School of Physical Sciences, University of Chinese Academy of Sciences, Beijing 100049, China.

[10]Songshan Lake Materials Laboratory, Dongguan, Guangdong 523808, China.

[11]National Institute of Biological Sciences, 7 Science Park Road, Zhongguancun Life Science Park, Beijing 102206, China.

[12]Beijing National Laboratory for Molecular Sciences, College of Chemistry and Molecular Engineering, Peking University, Beijing 100871, China.

[13]Biomedical Pioneering Innovation Center (BIOPIC), Peking University, Beijing 100871, China.

[14]Center for Life Sciences, Academy for Advanced Interdisciplinary Studies, Peking University, Beijing 100871, China.

†These authors contributed equally: Zhaoyi Zhai, Xue Bai, Bo Yan, Zehao Zhou, Fang Chen.

*Corresponding to: Fang Jiao (fang.jiao@iphy.ac.cn), Zhe Zhang (zzhang01@pku.edu.cn), Youwei Ai (aiyouwei@genetics.ac.cn), Yi Qin Gao (gaoyq@pku.edu.cn).

Supplementary figures

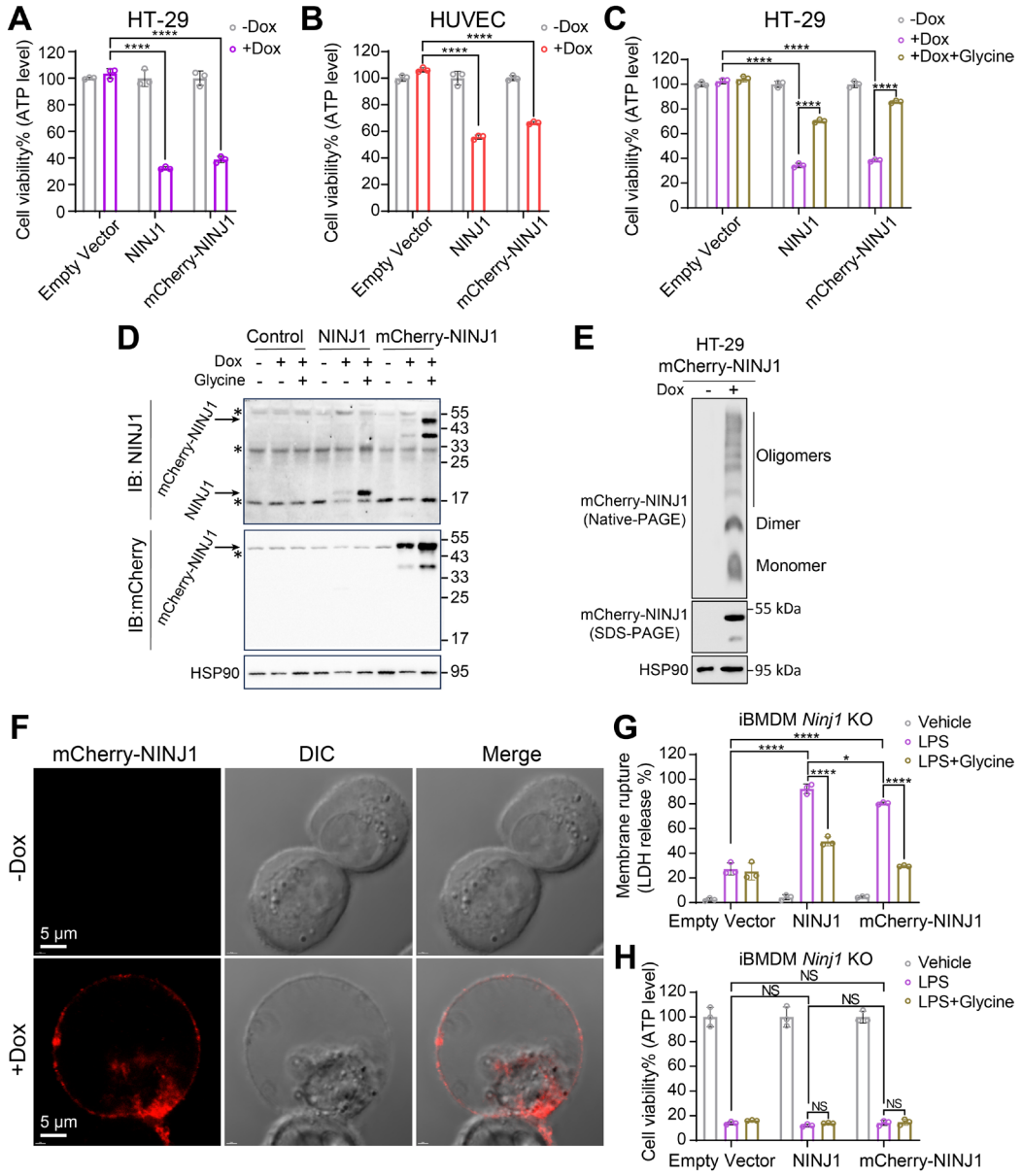

Fig. S1. **mCherry-NINJ1 exhibits plasma membrane rupture function**. (**A**) HT-29 empty vector, pLVX-NINJ1, and pLVX-mCherry-NINJ1 cells were treated with or without Dox for 48 h. Cell viability was assessed by ATP-based luminescence. Two-way ANOVA: ****P < 0.0001. (**B**) HUVEC empty vector, pLVX-NINJ1, and pLVX-mCherry-NINJ1 cells were treated with or without Dox for 48 h. Cell viability was assessed by ATP-based luminescence. Two-way ANOVA: ****P < 0.0001. (**C**) HT-29 empty vector, pLVX-NINJ1, and pLVX-mCherry-NINJ1 cells were treated with glycine (10 mM) with or without Dox for 48 h. Cell viability was assessed by ATP-based luminescence. Two-way ANOVA: ****P < 0.0001. (**D**) HT-29 empty vector, pLVX-NINJ1, and pLVX-mCherry-NINJ1 cells were treated as indicated for 24 h, and immunoblot analysis was performed to detect NINJ1 expression (asterisks indicate non-specific bands). (**E**) HT-29 pLVX-mCherry-NINJ1 cells were treated as indicated for 24 h. Native-PAGE analysis was used to assess NINJ1 oligomerization. (**F**) HT-29 pLVX-mCherry-NINJ1 cells were treated with or without Dox for 36 h. Confocal microscope was used to visualize mCherry-NINJ1 at the plasma membrane. Scale bar, 2 μm. (**G-H**) *Ninj1* KO iBMDMs reconstituted with NINJ1 or mCherry-NINJ1, and KO controls were electroporated with LPS (1 μg/mL) to induce pyroptosis,

followed by glycine treatment for 2 h. Plasma membrane rupture (PMR) was assessed by LDH release (**G**), and cell viability was determined by ATP levels (**H**). Two-way ANOVA: ns; *P = 0.0133; ****P < 0.0001.

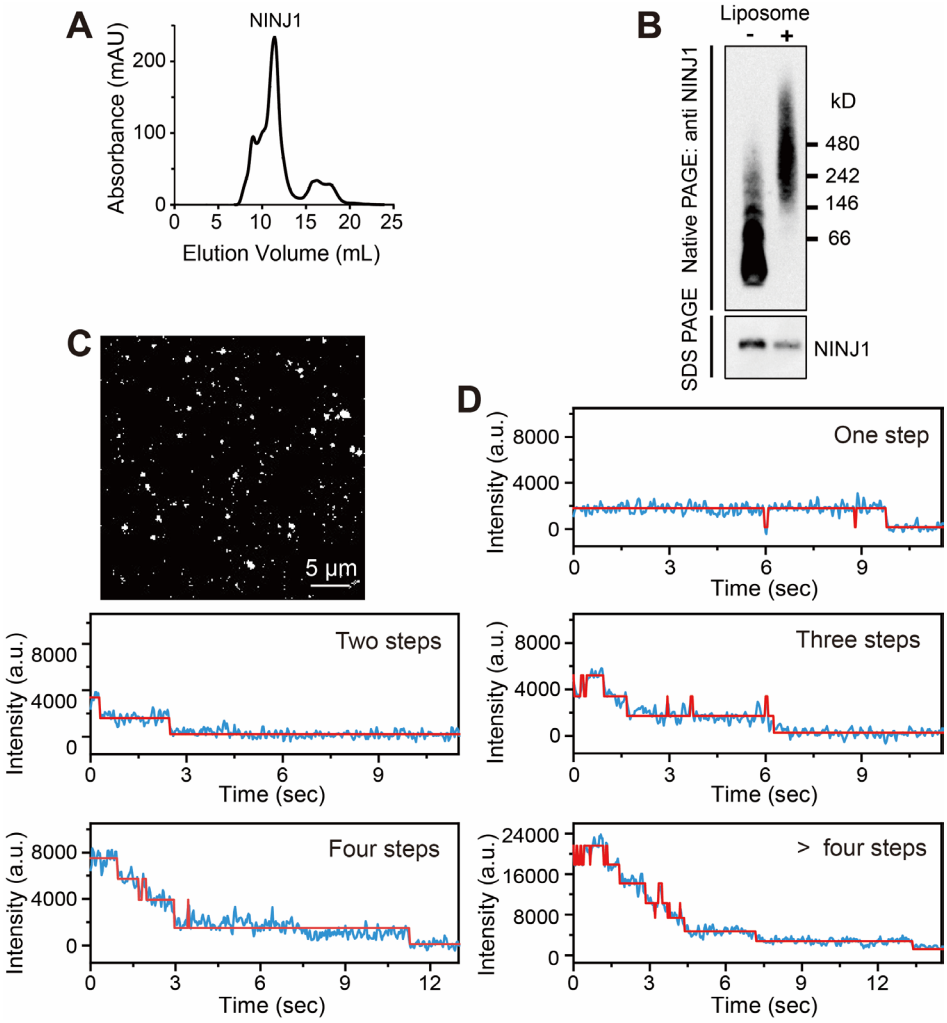

Fig. S2. Characterization of NINJ1 purification, oligomerization, and activity. (**A**) Size-exclusion chromatography (SEC) profile of purified human NINJ1 in C12E8. The x axis represents elution volume (mL), and the y axis represents absorbance at 280 nm. (**B**) Western blotting of NINJ1 with or without liposome (DOPC:DOPS 8:2). (**C, D**) Photobleaching analysis of single mCherry-NINJ1 complexes reveals the number of subunits. (**C**) Representative binary image of the selected fluorescent spots in the membrane milieu. (**D**) Time courses (blue) of fluorescent emission for mCherry-NINJ1 oligomers with fitting step curves (red). The number of subunits in the NINJ1 oligomer is essentially represented by the number of steps in the fitted curve.

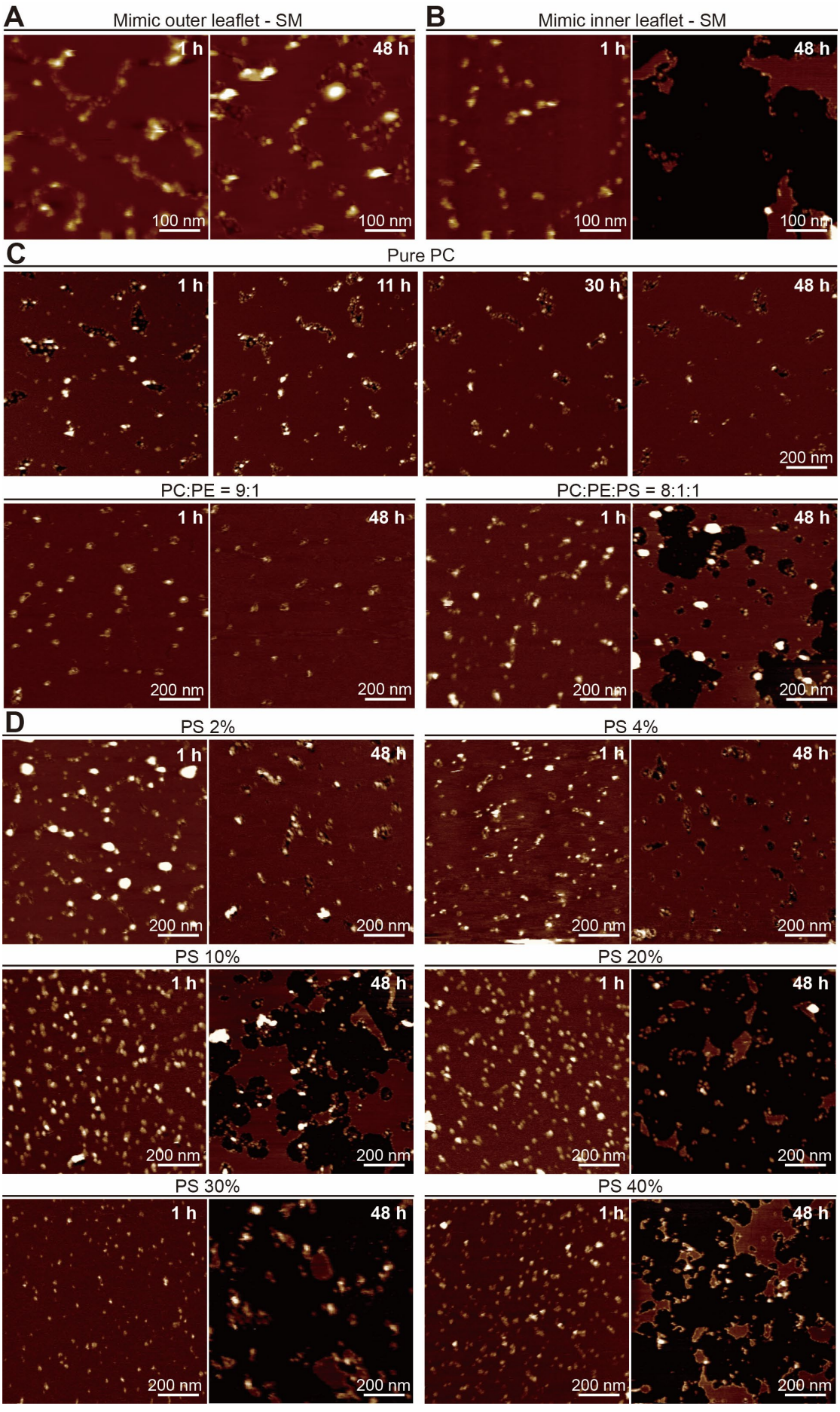
A
Mimic outer leaflet - SM
1 h
48 h
100 nm
100 nm
B
Mimic inner leaflet - SM
1 h
48 h
100 nm
100 nm
C
Pure PC
1 h
11 h
30 h
48 h
200 nm
PC:PE = 9:1
1 h
48 h
200 nm
200 nm
PC:PE:PS = 8:1:1
1 h
48 h
200 nm
200 nm
D
PS 2%
1 h
48 h
200 nm
200 nm
PS 4%
1 h
48 h
200 nm
200 nm
PS 10%
1 h
48 h
200 nm
200 nm
PS 20%
1 h
48 h
200 nm
200 nm
PS 30%
1 h
48 h
200 nm
200 nm
PS 40%
1 h
48 h
200 nm
200 nm

Fig. S3. AFM images of NINJ1 reconstituted in lipid membranes with varying compositions. (**A-C**) AFM images showing reconstituted NINJ1 in lipid membranes of simulated (**A**) outer leaflet in absence of SM, (**B**) inner leaflet in absence of SM, (**C**) pure PC, 9:1 PC:PE, 8:1:1 PC:PE:PS, after 1 and 48 h of incubation. Top of panel C shows *in-situ* images with incubation time of 1, 11, 30 and 48 h. Z scale bar: 10 nm. (**D**) AFM images showing reconstituted NINJ1 in lipid membranes of 98:2, 96:4, 90:10, 80:20, 70:30 and 60:40 PC:PS, after 1 and 48 h of incubation. Z scale bar: 10 nm.

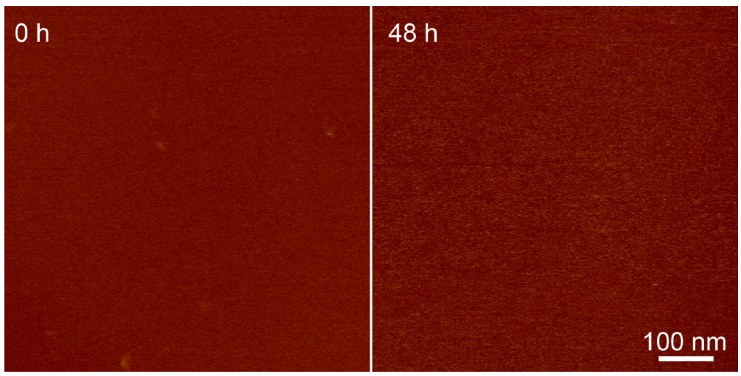

Fig. S4. AFM images of reconstituted DOPC:DOPS (8:2) SLBs from a control experiment, showing stability and no membrane disruption over 48 hours.

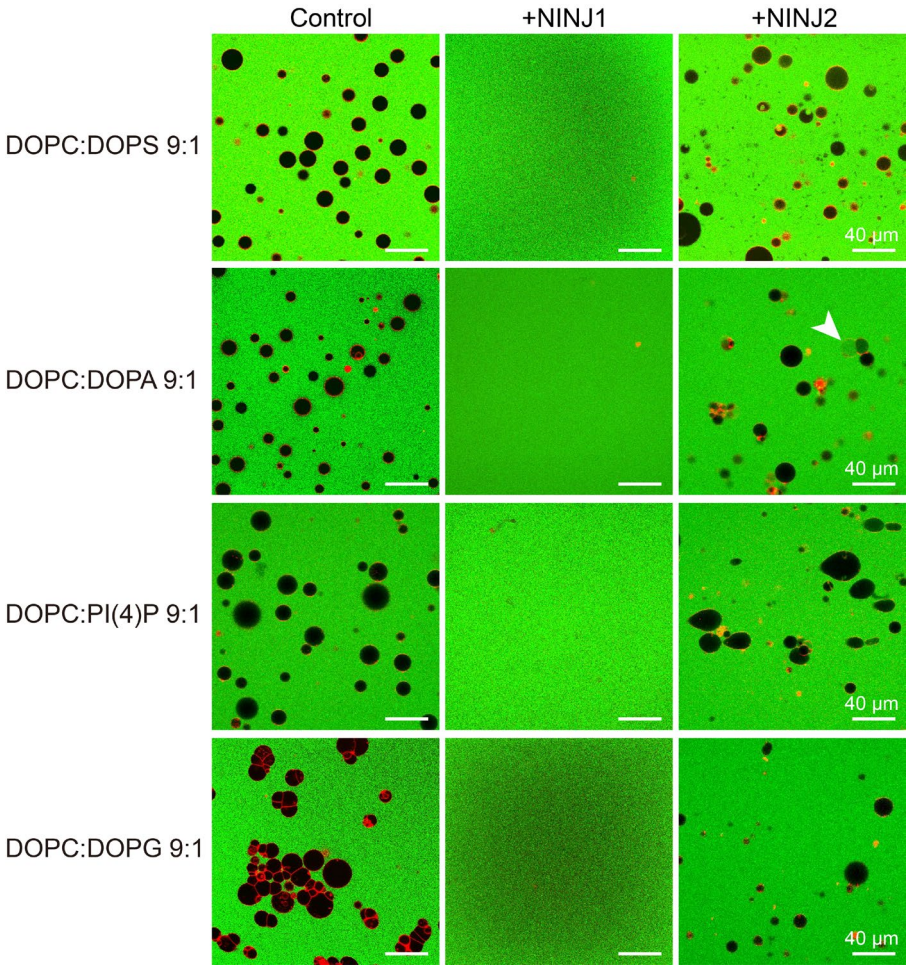

Fig. S5. Lipid composition–dependent GUV leakage induced by NINJ1 and NINJ2. Merged confocal fluorescence microscopy images of GUVs composed of negatively charged binary lipid mixtures (DOPC:DOPS 9:1, DOPC:DOPA 9:1, DOPC:PI(4)P 9:1, and DOPC:DOPG 9:1), labeled with a rhodamine lipid probe (red, 0.1%) and suspended in buffer containing FITC–Dextran (20 kDa, green). Upon addition of 600 nM NINJ1, GUVs containing negatively charged lipids were disrupted and disappeared. In contrast, NINJ2 did not induce GUV dissolution across any tested lipid compositions. Occasionally, slight distortions were observed in 9:1 DOPC:PI(4)P GUVs. A small percentage of negatively charged GUVs exhibited leakage upon NINJ2 treatment. White arrowheads indicate GUVs that leaked following NINJ2 exposure.

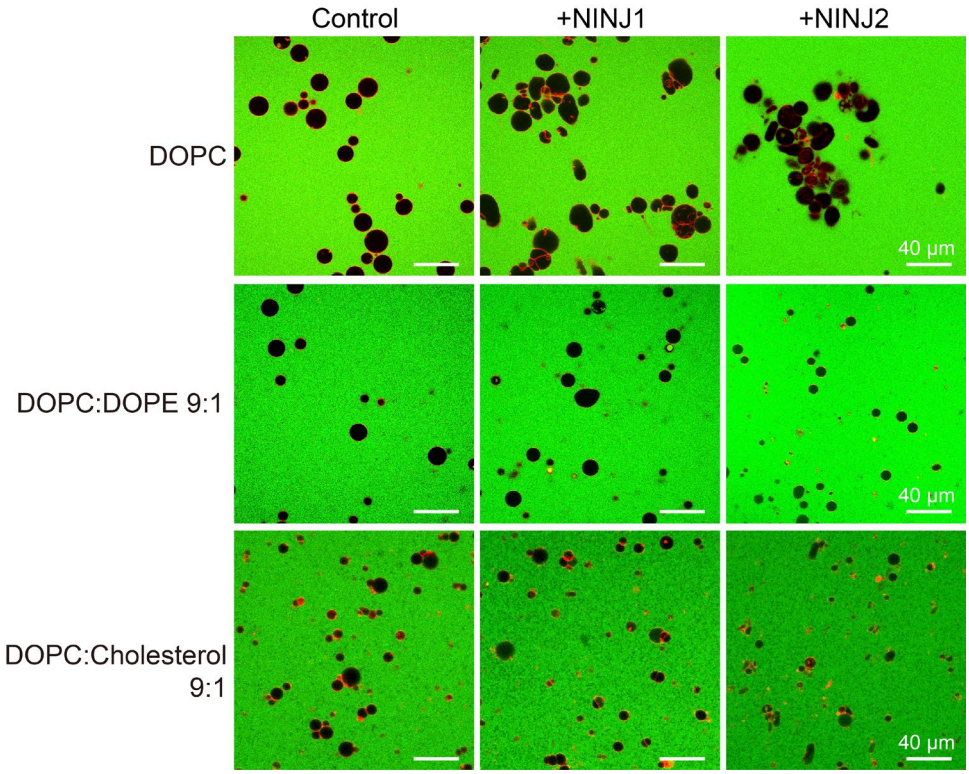

Fig. S6. Lipid composition–dependent GUV leakage induced by NINJ1 and NINJ2. Merged confocal fluorescence microscopy images of GUVs composed of DOPC or binary lipid mixtures (DOPC:DOPE 9:1, DOPC:cholesterol 9:1), labeled with a rhodamine lipid probe (red, 0.1%) and suspended in buffer containing FITC–Dextran (20 kDa, green). Upon addition of 600 nM NINJ1 or NINJ2, neither protein induced rupture or leakage of neutral GUVs; only partial morphological distortion was observed.

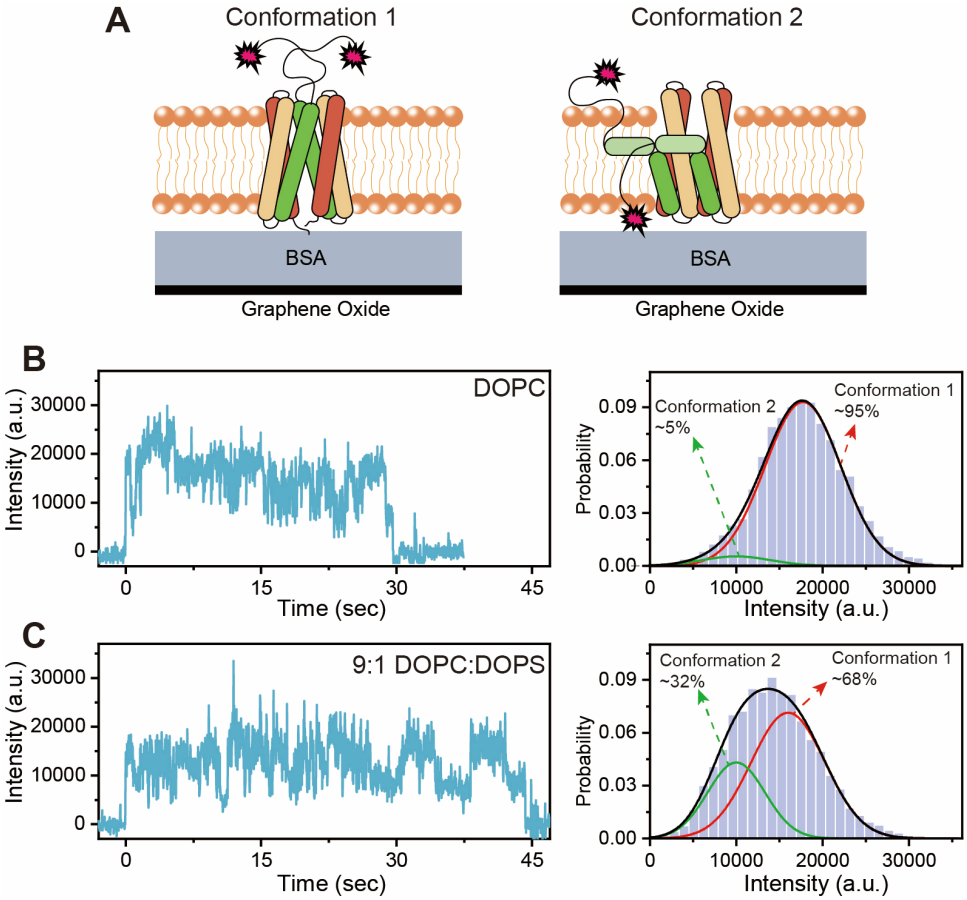

Fig. S7. Single molecule SIFA (smSIFA) measurement of NINJ1. (**A**) Schematics of smSIFA experiments distinguishing two conformations of NINJ1 N-terminus. (**B-C**) Representative fluorescence traces (left) and corresponding statistical histograms of NINJ1 N-terminus on SLBs composed of (**B**) pure DOPC and (**C**) 9:1 DOPC:DOPS.

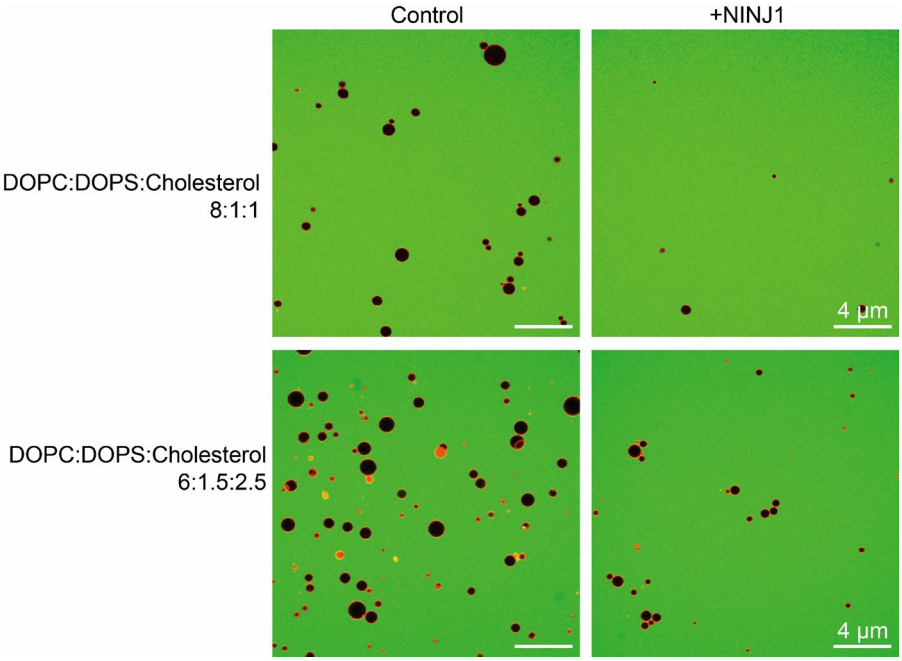

Fig. S8. Lipid composition–dependent GUV leakage induced by NINJ1. Merged confocal fluorescence microscopy images of GUVs composed of lipid mixtures (DOPC:DOPS:Cholesterol 8:1:1, and 6:1.5:2.5), labeled with a rhodamine lipid probe (red, 0.1%) and suspended in buffer containing FITC–Dextran (20 kDa, green). Upon addition of 600 nM NINJ1, a portion of GUVs were disrupted and disappeared.

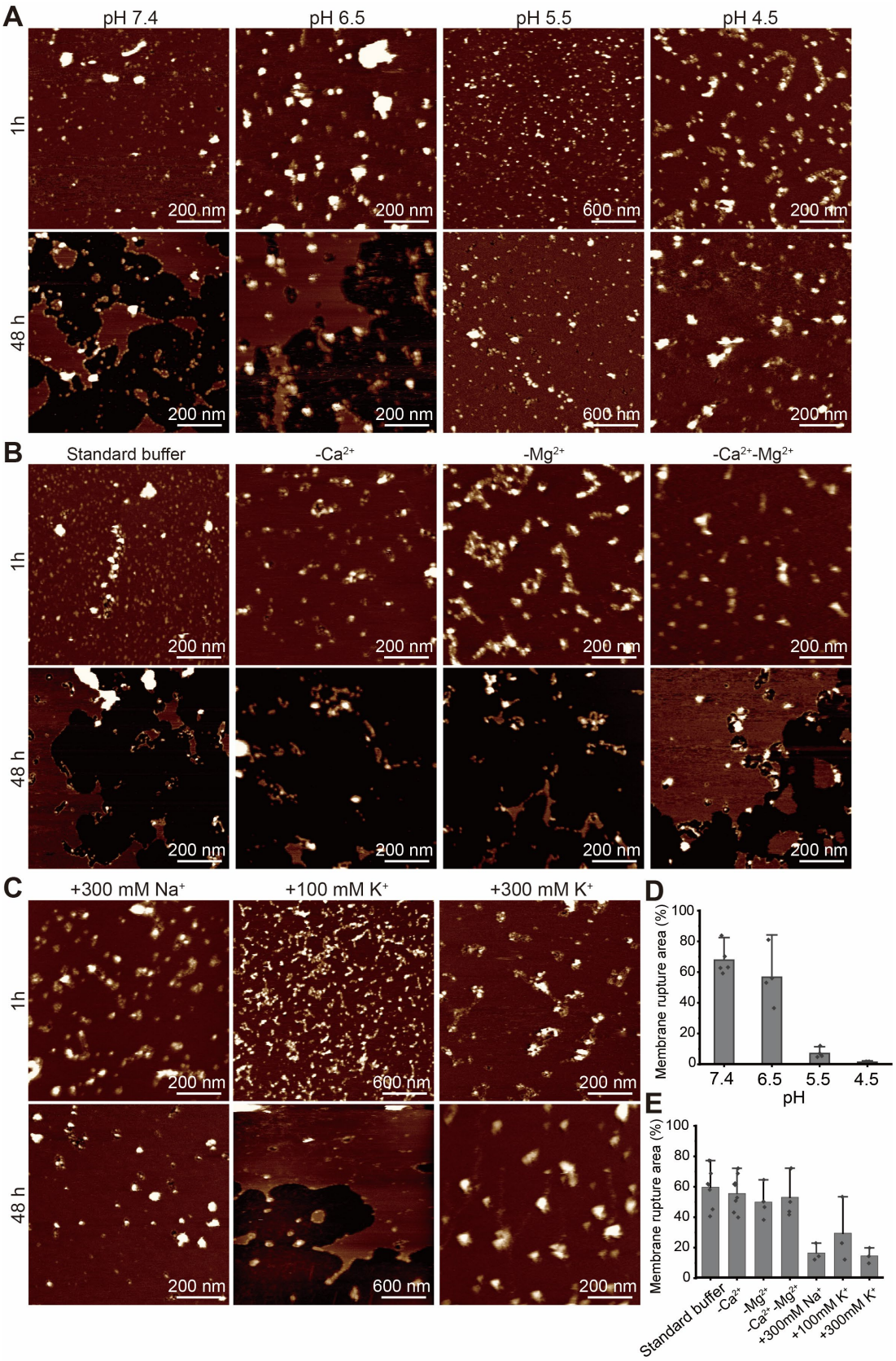

Fig. S9. Effects of pH and mono- and di-valent salts on NINJ1-mediated PMR. (**A-C**) AFM images of incubating reconstituted NINJ1 in 8:1:1 PC:PE:PS lipid membrane for 1- and 48-h under buffer conditions: (**A**) pH 7.4, 6.5, 5.5, and 4.5; (**B**) standard buffer (25 mM HEPES-NaOH, pH 7.4, 150 mM NaCl, 1 mM $CaCl_2$ and 1 mM $MgCl_2$) and buffers with either $CaCl_2$ or 1 mM $MgCl_2$ omitted, or both

removed; (**C**) standard buffer with the addition of 300 mM NaCl, 100 mM KCl, and 300 mM KCl, respectively. Z scale bar: 10 nm. (**D, E**) Rupture areas of lipid membrane induced by reconstituted NINJ1 after 48 h incubation under conditions (**D**) 8:1:1 PC:PE:PS membranes at pH 7.4, 6.5, 5.5 and 4.5, (**E**) 8:1:1 PC:PE:PS membranes in various buffer solutions compared with standard buffer (25 mM HEPES-NaOH, pH 7.4, 150 mM NaCl, 1 mM $CaCl_2$ and 1 mM $MgCl_2$).

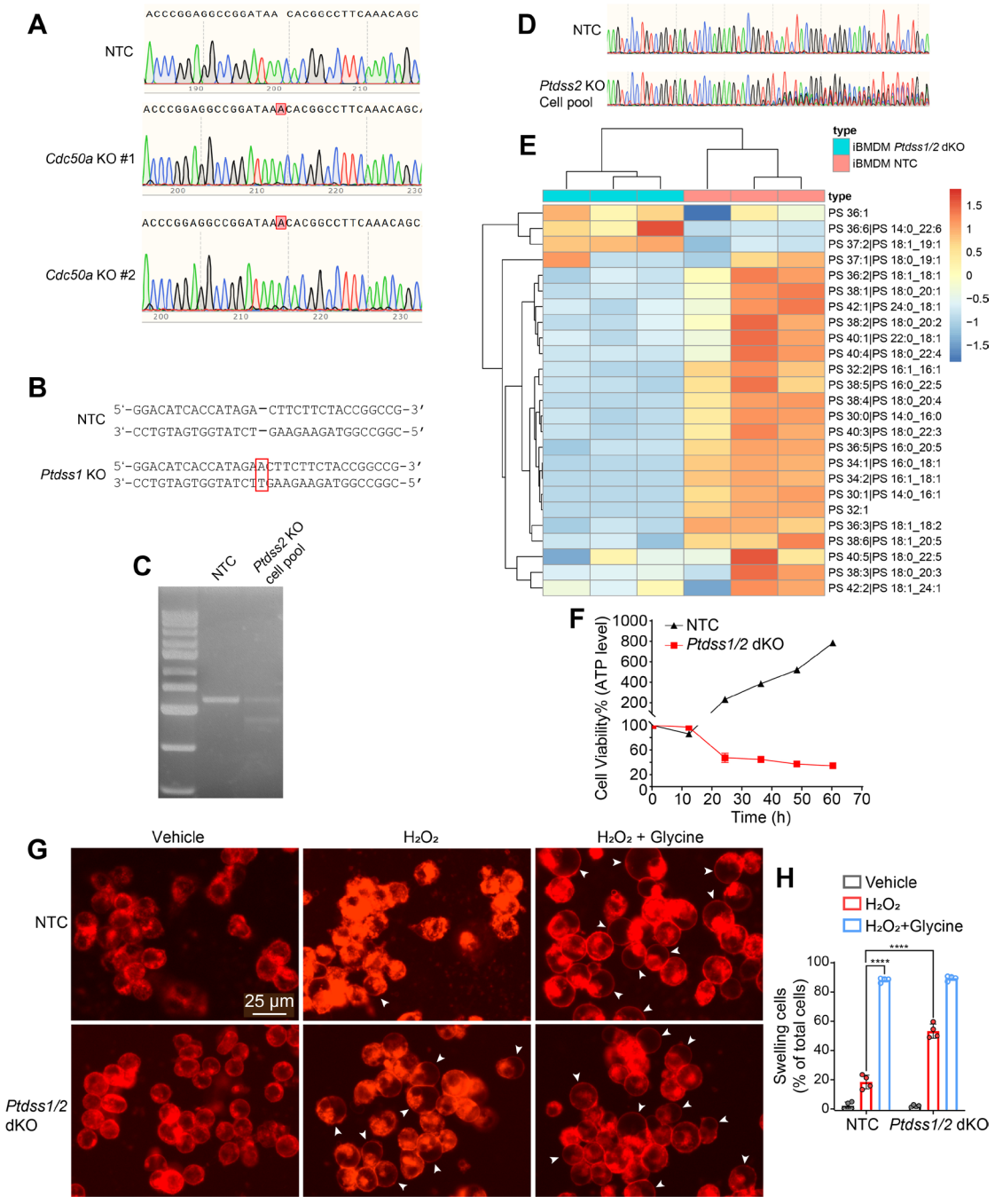

Fig. S10. Generation and H_2O_2 stimulation of iBMDM *Cdc50a* KO and *Ptdss1/2* dKO cells. (**A**) Sanger sequencing chromatograms of WT iBMDMs (non-targeting control gRNA) and *Cdc50a* knockout clones (#1 and #2, generated using two distinct gRNAs). *Cdc50a* KO clones show a base pair insertion in the coding region. (**B**) A base pair insertion in the coding region of *Ptdss1* gene caused frameshift mutation in iBMDM *Ptdss1* KO cells. WT cells infected with a non-targeting control gRNA. (**C**) T7 endonuclease I (T7E1) assay confirming the editing efficiency of *Ptdss2*-targeting gRNA in *Ptdss1* KO iBMDMs. (**D**) Sanger sequencing traces around the *Ptdss2* gRNA target site show multiple overlapping peaks, indicating heterogeneity and mutation at the locus. (**E**) Heatmap of phosphatidylserine (PS) species measured by lipidomic analysis in WT and *Ptdss1/2* dKO iBMDMs 12 h after phosphatidylserine (POPS) withdrawal. Each column represents a biological replicate (n = 3 per group). (**F**) iBMDM NTC

cells and *Ptdss1/2* dKO cells were cultured in the presence of POPS to maintain cell survival. Time 0 indicates the time point POPS is withdrawn from the culture medium. Cell viability was determined 3 days after POPS withdrawal (repeat experiments, n=3). (**G**) WT and *Ptdss1/2* dKO iBMDMs were treated with H_2O_2 (15 mM) for 2 h with or without 20 mM glycine. Cells were stained with Nile Red. (**H**) Quantification of swelling cells as a percentage of total cells (n = 4). Two-way ANOVA: ****$P < 0.0001$. Vehicle treatment served as control. All data are presented as mean ± s.d. Representative images are from at least three independent experiments unless otherwise indicated.

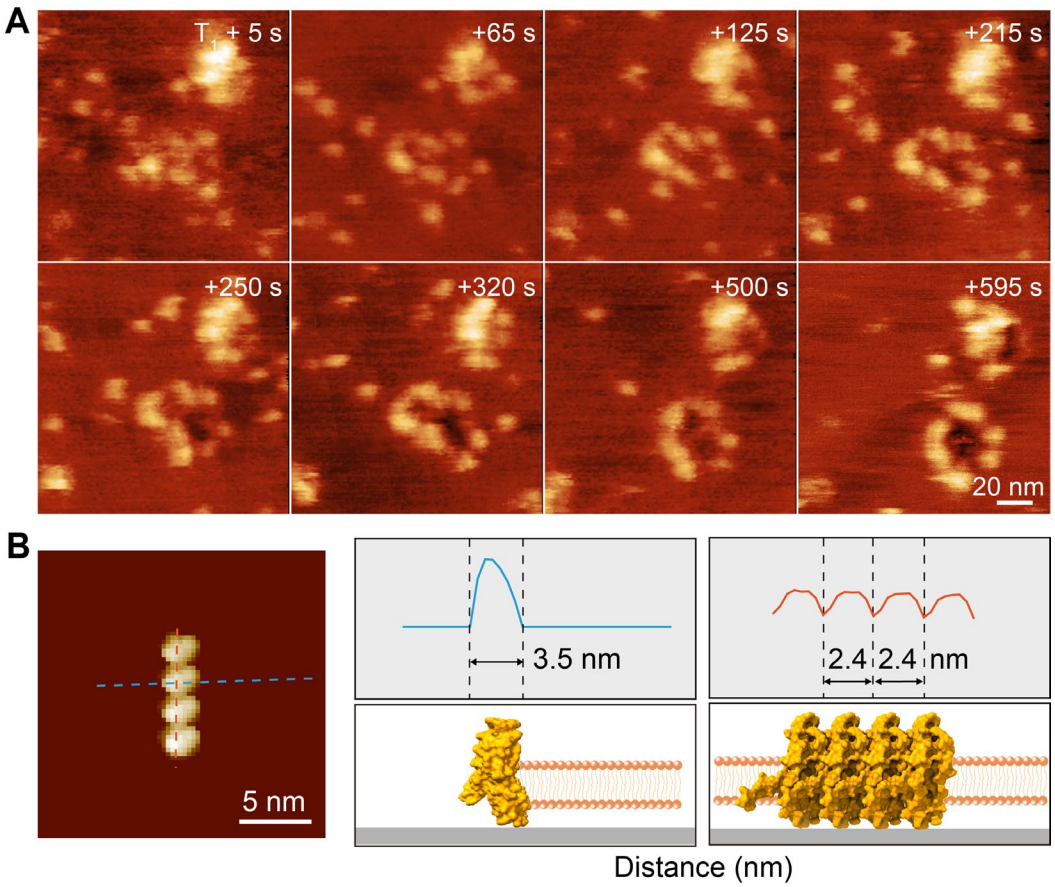

Fig. S11. NINJ1 pore formation. (**A**) HS-AFM frames depicting NINJ1 mediated pore-formation. (**B**) Left, simulated AFM images based on the resolved structure from PDB 8cqr. Right, height profiles correspond to the dashed lines, alongside their respective schematic representations.

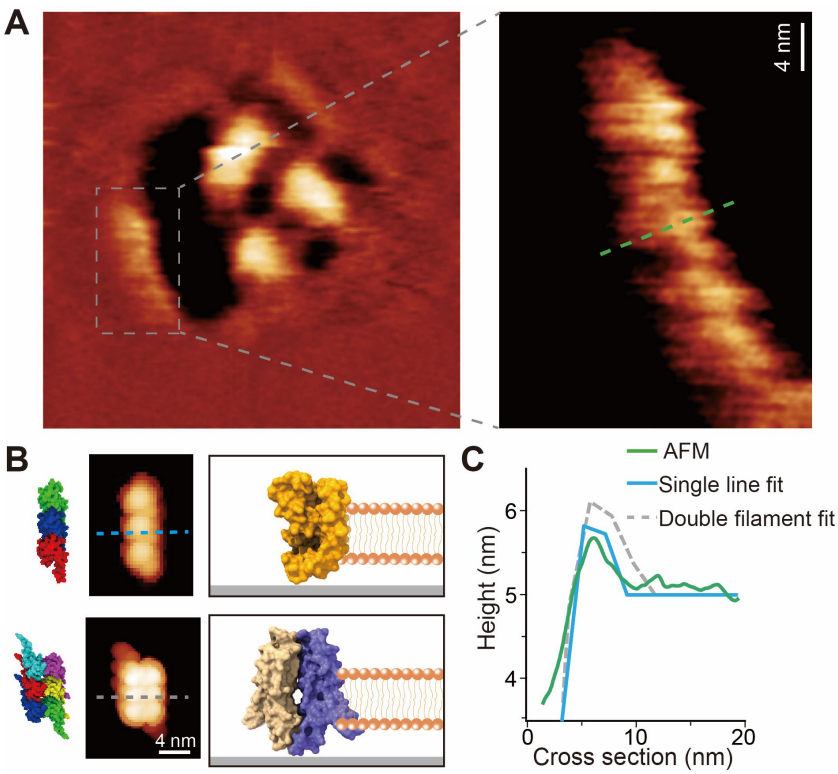

Fig. S12. High-resolution AFM imaging and structural simulation of NINJ1 pores. (**A**) High-resolution AFM image of NINJ1 pores with a zoomed-in view of the pore rim. (**B**) Simulated AFM images of single-linearly packed and back-to-back double filaments of NINJ1 oligomers, based on the resolved structures of PDB 8uip (single filament) and PDB 8cqr (double filament). (**C**) Section profiles along the dashed lines in panels (**A**) and (**B**) highlight the rim features of NINJ1 pores corresponding to single-linearly packed oligomers.

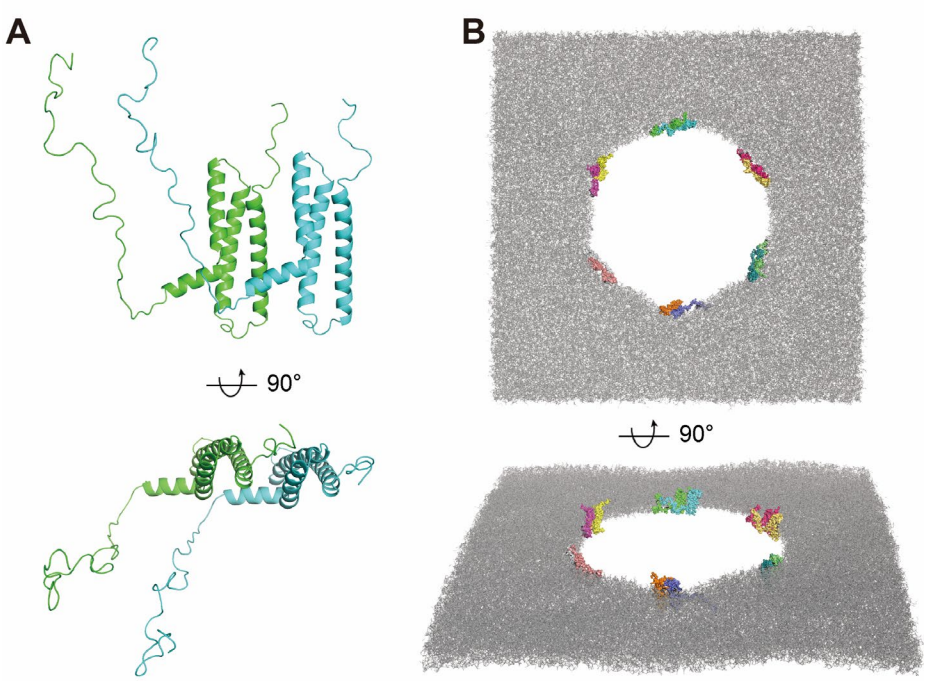

Fig. S13. MD of stable membrane pore formed by NINJ1 dimers. (**A**) Structure of the NINJ1 dimer. (**B**) Coarse-grained MD simulation based on NINJ1 dimeric structure, with positional restraints applied to residues 39-142 throughout the simulation for 1 μs. Each NINJ1 monomer is shown in a different color for clarity.

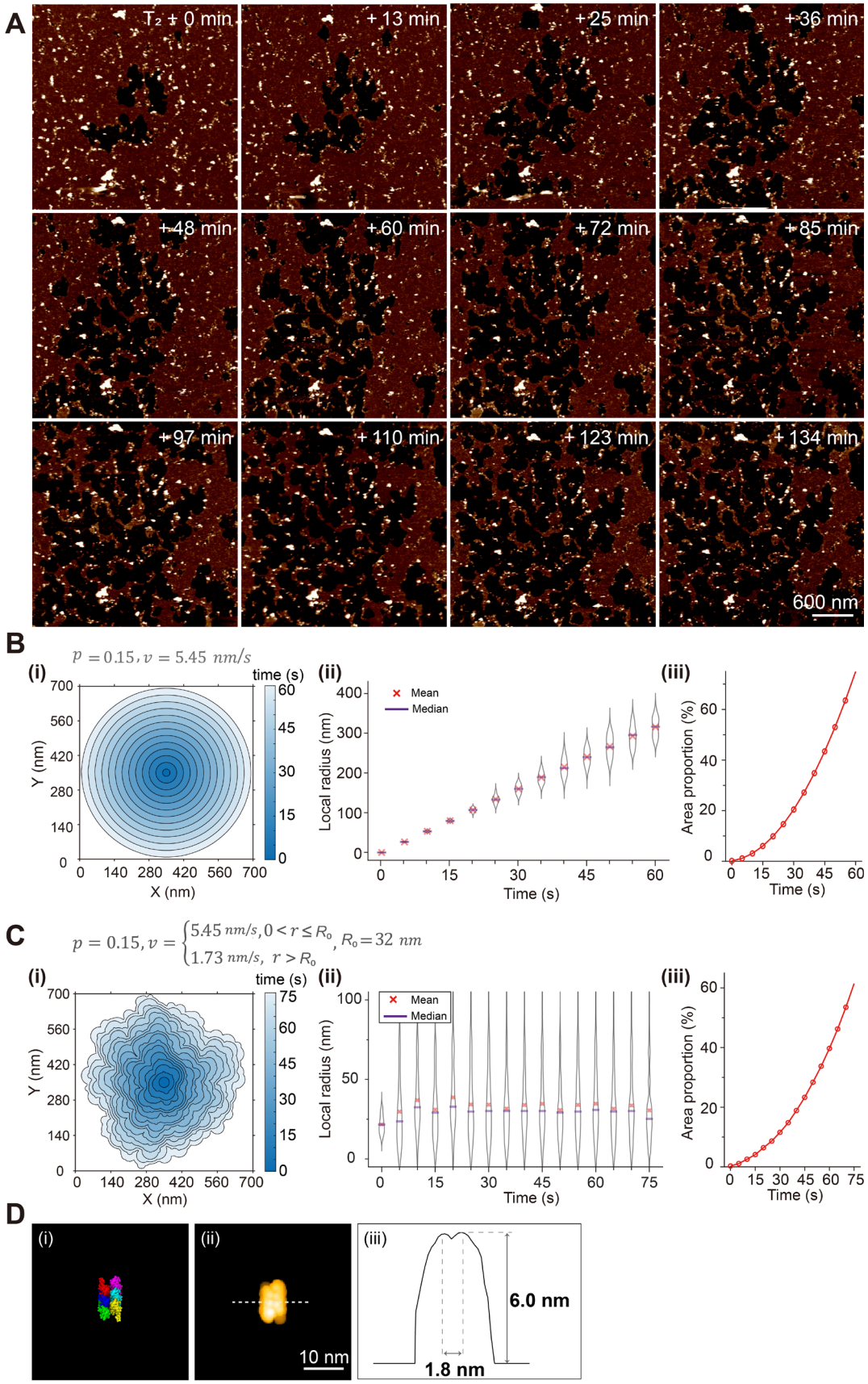

Fig. S14. NINJ1 pore enlargement and simulated AFM image. (**A**) Conventional AFM images captured by extended periods (T_2) of reconstituted NINJ1 in membrane of 8:1:1 PC:PE:PS. (**B**) Travelling-wave model with a constant expansion rate. The simulated wave expands isotopically,

generating a concentric-circle-shaped contour map (i). The pore area proportion exhibits parabolic growth (iii), with the curvature radius increasing linearly (ii). (**C**) Travelling-wave model with the expansion rate constrained by curvature (R_0 = 32 nm). The simulated wave expands anisotropically (i), maintaining a constant local rim curvature (ii). Meanwhile, the proportion of the pore area shows quadratic growth (iii). (**D**) (i, ii) Simulated AFM image based on the resolved double filament structure (PDB 8sza); (iii) section profile of the double filament shown in panel (ii).

Legends of supplementary videos:

Movie S1. All-atom molecular dynamics simulation of NINJ1 monomer adopting the N-in inactive conformation from the inactive state (PDB 9bia) in the membrane.

Movie S2. All-atom molecular dynamics simulation of NINJ1 dimer adopting the N-in inactive conformation from the inactive state (PDB 9bia) in the membrane.

Movie S3. All-atom molecular dynamics simulation of NINJ1 tetramer adopting the N-in inactive conformation from the inactive state (PDB 9bia) in the membrane.

Movie S4. Laser scanning confocal microscopy (LSCM) time-lapse imaging showing GUV disruption or disappearance induced by NINJ1. The GUV composition is DOPC:DOPS:Liss rhod PE(18:1) = 9:1:0.01. Green represents FITC-Dextran (20 kDa) in the solution and red represents 18:1 Liss rhod PE.

Movie S5. Wide-field time-lapse imaging through structured illumination microscopy showing GUV disruption or disappearance induced by NINJ1. The GUV composition is DOPC:DOPA:Liss rhod PE(18:1) = 9:1:0.01. Blue represents Cy5 labeled NINJ1, green represents FITC-Dextran (20 kDa) in the solution and red represents 18:1 Liss rhod PE.

Movie S6. Laser scanning confocal microscopy (LSCM) time-lapse imaging showing GUV disruption or disappearance induced by NINJ1. The GUV composition is DOPC:PI(4)P:Liss rhod PE(18:1) = 9:1:0.01. Green represents FITC-Dextran (20 kDa) in the solution and red represents 18:1 Liss rhod PE.

Movie S7. Laser scanning confocal microscopy (LSCM) time-lapse imaging showing GUV disruption or disappearance induced by NINJ1. The GUV composition is DOPC:DOPG:Liss rhod PE(18:1) = 9:1:0.01. Green represents FITC-Dextran (20 kDa) in the solution and red represents 18:1 Liss rhod PE.

Movie S8. *In situ* HS-AFM imaging showing NINJ1 mediated pore-formation in SLB.

Movie S9. Coarse-grained molecular dynamics simulation of a pre-formed hole in the lipid membrane (DOPC:DOPE:DOPS=8:1:1), without any NINJ1 protein, and the hole spontaneously closes within 100 ns.

Movie S10. *In situ* HS-AFM imaging showing the NINJ1 pore enlargement in SLB.

Movie S11. Zoomed-in HS-AFM frames showing the formation of membrane fragments following pore expansion.